Redundancy Resolution of Wire-Actuated Parallel Manipulators Considering Contact Forces in Machining Applications

Maryam Agahi[1], Leila Notash[2]

[1]Department of Mechanical and Materials Engineering, Queen's University, agahi@me.queensu.ca

[2]Department of Mechanical and Materials Engineering, Queen's University, notash@me.queensu.ca

Abstract

In the work presented, the redundancy resolution of planar wire-actuated parallel manipulators is investigated at the torque level using analytical methods in order to perform desirable tasks. As an example application where there are forces and moments at the mobile platform, wire-actuated manipulators are used in machining operations. The kinematic analysis and trajectory planning of the mobile platform are investigated taking into account the depth of cut and the geometry of the cutting surface. Considering the actuation redundancy, wire diameter and material recommendations are made for a given cutting force in the machining process. Analytical methods are used in the formulations in order to minimize the norm of actuator forces/torques such that the minimum required cutting force is achieved. The effectiveness of the presented approaches is studied through a simulation of an example planar wire-actuated manipulator.

Keywords: Wire-actuated parallel manipulators, redundancy resolution, machining applications

1. INTRODUCTION

In closed-loop manipulators, the manipulator is redundantly actuated if the number of actuators is greater than the degrees of freedom of the manipulator, where for a given end effector trajectory and external forces/moments, an infinite number of actuator forces/torques exists. Redundant manipulators can use their degree(s) of redundancy to satisfy additional desirable task(s), e.g., to avoid actuator torque/force limits, reduce impact, and improve reliability, safety and performance of the manipulator. A parallel manipulator consists of a mobile platform (end effector) connected to a fixed base by several branches/legs/limbs/wires. If all links of a manipulator are constrained to move in a plane or in parallel planes, then the manipulator is called planar. Wire-actuated parallel manipulators are a special kind of parallel manipulator with the advantage of being light weight, reconfigurable and transportable, and allowing high speed motion and a larger workspace compared to conventional manipulators. Wires can only apply force in the form of tension. Therefore, to design a fully controllable wire-actuated parallel manipulator, the manipulator has to be redundantly actuated. Thus, to keep positive tension in all wires, at least $n + 1$ wires are required for a manipulator with n degrees of freedom (DOF) [1-4].

Various techniques have been applied for redundancy resolution of redundant manipulators. When resolving redundancy at the torque level, given the external forces and moments on the mobile platform, because of the existence of infinite solutions for the actuator forces/torques some actuator forces/torques (referred to as the homogenous solution) result in zero forces/moments at the mobile platform. The homogenous solution can be used to achieve desirable performance criteria, improve the performance, and have a fail-safe manipulator. The kinematic, dynamic and stiffness analyses, as well as, the design of wire-actuated manipulators have been studied, e.g., [1-9]. Some researchers, e.g., [6, 8, 9], investigated how to design positive tension controllers for wire-actuated manipulators to follow prescribed trajectories. Kawamura et al. [1] used non-linear elasticity of wires and the internal forces arising from the redundant actuation to reduce the undesirable vibrations of wire-actuated parallel manipulators.

A wire-actuated manipulator can be used for various applications similar to those of solid-link parallel manipulators. Depending on the application of the manipulator, e.g., assembly, machining and pick-and-place applications, knowing the required loads on the mobile platform is of great interest in order to minimize the wire tensions, motor torques and power consumption. It is also beneficial to know whether the mobile platform can maintain its position and orientation (pose) while providing the required forces/moments at the mobile platform. In the presented work, a wire-actuated manipulator is used in machining applications. Then, for a given machining trajectory and cutting force, the trajectory of the mobile platform is determined. Analytical methods are utilized to find the minimum norm tension in the wires corresponding to the desired cutting force. Some of the challenges associated with the redundancy resolution of wire-actuated parallel manipulators, including positive tension requirement in each wire, infinite inverse dynamic solutions, and using fast-computation abilities when utilizing analytical methods are addressed. Since wires are more flexibile than rigid links, possible vibration of wires and the mobile platform is a concern when dealing with wire-actuated manipulators. Thus, the investigation of vibration of wire-actuated manipulators is important for applications requiring high system stiffness or bandwidth [10]. These vibrations could be reduced by increasing the internal forces (i.e., the pre-tension in the wires) of wire-actuated parallel manipulators using the homogenous solution in order to provide more stable motion. To achieve precise path tracking of the platform while damping out the undesirable mechanical vibrations, intelligent control system, including sensor feedback control, could also be developed. It should be noted, however, that vibration analysis is beyond the scope of the work presented.

The modelling of an example planar wire-actuated parallel manipulator is presented in Section 2, where Section 2.1 corresponds to the kinematic and dynamic analyses, Section 2.2 covers the trajectory planning of the mobile platform and the kinematics of the tool tip, and Section 2.3 provides the force relationships and power requirements in cutting operations. The simulation results are reported in Section 3. The article concludes with Section 4.

2. MODELLING

In this section, the redundancy resolution of a planar wire-actuated parallel manipulator shown in Figure 1(a) is investigated at the dynamic level. Figure 1(b) shows the coordinates and parameters used for the analysis of a planar wire-actuated parallel manipulator. The fixed coordinate system Ψ(X, Y), located at O, is attached to the base, while the moving coordinate system, Γ(X′, Y′), is attached to the mobile platform at its centre of mass P with position vector of $\mathbf{x}_P = [x, y]^T$ in Ψ(X, Y). All vector expressions will be in the base reference frame unless otherwise stated. The position of the base attachment point of each wire (anchor) A_i is $\mathbf{a}_i = [a_{ix}, a_{iy}]^T$, $r_{Bi/P}$ is the distance between the attachment point of wire i on the mobile platform B_i and point P, θ_i is the orientation of the position vector $\mathbf{r}_{Bi/P}$ in Γ(X′, Y′), and $\mathbf{l}_i = [l_i\cos\alpha_i, l_i\sin\alpha_i]^T$ is the vector of the magnitude and direction of each wire.

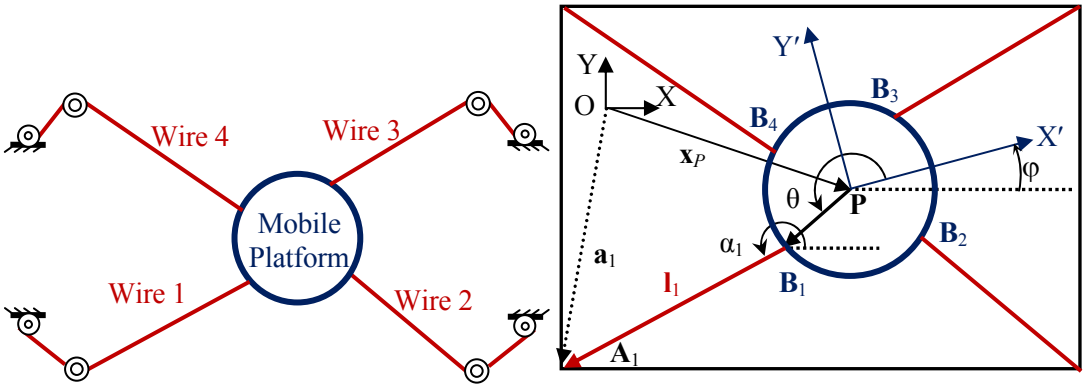

Figure 1. (a) Example planar 3-DOF wire-actuated parallel manipulator, (b) coordinates and variables.

Figure 2(a) illustrates the schematics of a planar wire-actuated manipulator used in cutting applications, and Figure 2(b) shows a schematic representation of orthogonal cutting, wherein the cutting edge is perpendicular to the cutting velocity.

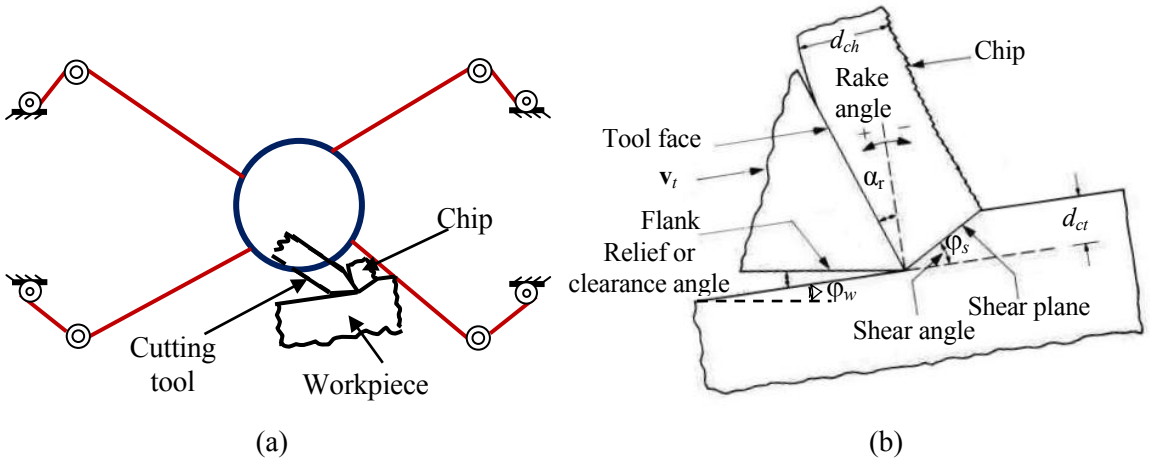

Figure 2. (a) Example application of wire-actuated parallel manipulator in cutting operations, (b) schematic representation of orthogonal cutting.

2.1. Kinematic and Dynamic Analyses

The inverse velocity solution that relates the mobile platform velocity $\dot{\mathbf{x}} = [\dot{x}, \dot{y}, \dot{\varphi}]^T$ to the wire length rates $\dot{\mathbf{l}} = [\dot{l}_1, \ldots, \dot{l}_n]^T$ is given by

$$\begin{bmatrix} \dot{l}_1 \\ \vdots \\ \dot{l}_n \end{bmatrix} = -\begin{bmatrix} c_1 & s_1 & -r_{B_1/P}\, s(\varphi + \theta_1 - \alpha_1) \\ \vdots & \vdots & \vdots \\ c_n & s_n & -r_{B_n/P}\, s(\varphi + \theta_n - \alpha_n) \end{bmatrix} \begin{bmatrix} \dot{x} \\ \dot{y} \\ \dot{\varphi} \end{bmatrix} = -\mathbf{J} \begin{bmatrix} \dot{x} \\ \dot{y} \\ \dot{\varphi} \end{bmatrix} \tag{1}$$

where c_i, s_i and $s(\varphi + \theta_i - \alpha_i)$, $i = 1, \ldots, n$, stand for $\cos\alpha_i$, $\sin\alpha_i$ and $\sin(\varphi + \theta_i - \alpha_i)$, respectively, φ is the orientation of the mobile platform, n ($n \geq 4$) is the number of wires, and the Jacobian matrix $\mathbf{J}$ is the negative of the coefficient of the mobile platform velocity.

Considering the free-body diagram of the mobile platform shown in Figure 3(a), the dynamic force and moment balances can be written as

$$\begin{aligned} \mathbf{J}^T \begin{bmatrix} \tau_1 \\ \vdots \\ \tau_n \end{bmatrix} &= \begin{bmatrix} m & 0 & 0 \\ 0 & m & 0 \\ 0 & 0 & I_z \end{bmatrix} \begin{bmatrix} \ddot{x} \\ \ddot{y} \\ \ddot{\varphi} \end{bmatrix} - \begin{bmatrix} 0 \\ -mg \\ 0 \end{bmatrix} - \begin{bmatrix} F_{ext_x} \\ F_{ext_y} \\ M_{ext_z} \end{bmatrix} \\ &= \mathbf{M}\ddot{\mathbf{x}} - \mathbf{g} - \mathbf{W} \end{aligned} \tag{2}$$

where m and I_z are the mass and moment of inertia of the mobile platform respectively, $[\tau_1, \ldots, \tau_n]^T$ is the vector of wire tensions, F_{ext_x} and F_{ext_y} are the components of the external force $\mathbf{F}_{ext}$, M_{ext_z} is the external moment acting on the mobile platform, $\mathbf{M}$ is the inertia matrix, $\ddot{\mathbf{x}} = [\ddot{x}, \ddot{y}, \ddot{\varphi}]^T$ is the vector of linear and angular accelerations of the mobile platform, $\mathbf{g}$ is the vector of gravitational force with $g = 9.81$ m/s^2, and $\mathbf{W}$ represents the external forces and moments (wrench).

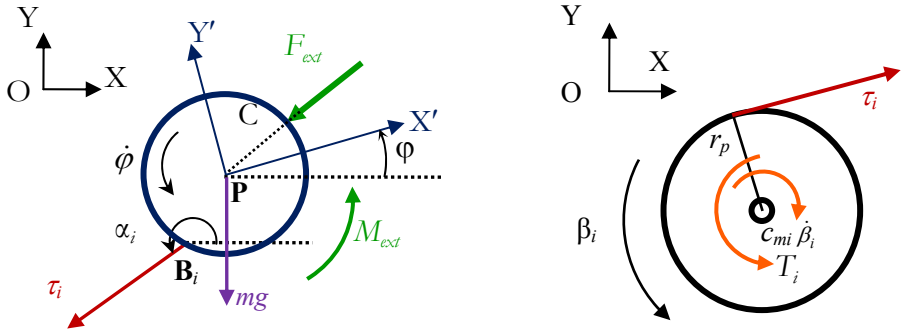

(a) (b)

Figure 3. (a) Free-body diagram of mobile platform, (b) free-body diagram of pulley of wire i.

Considering the free-body diagram of the pulleys shown in Figure 3(b), the actuators dynamics is expressed as

$$\begin{bmatrix} T_1 \\ \vdots \\ T_n \end{bmatrix} = \begin{bmatrix} r_{p_1}\tau_1 \\ \vdots \\ r_{p_n}\tau_n \end{bmatrix} + \begin{bmatrix} c_{m_1} & & 0 \\ & \ddots & \\ 0 & & c_{m_n} \end{bmatrix} \dot{\boldsymbol{\beta}} + \begin{bmatrix} I_{p_1} & & 0 \\ & \ddots & \\ 0 & & I_{p_n} \end{bmatrix} \ddot{\boldsymbol{\beta}} \tag{3}$$

where T_i is the torque motor i exerts, r_{pi} is the radius of spool i, c_{mi} is the viscous damping coefficient at motor shaft i, I_{pi} is the moment of inertia of spool i, $\boldsymbol{\beta}$, $\dot{\boldsymbol{\beta}}$ and $\ddot{\boldsymbol{\beta}}$ are respectively the vectors of spool rotations, angular velocity and angular acceleration. The angular velocities of spools are related to the wire length rates as:

$$\dot{\beta}_i = -\frac{1}{r_{p_i}} \dot{l}_i \,, \; i = 1, \ldots, n \tag{4}$$

where β_i is the rotation of spool i and $\dot{l}_i$ is given by equation (1). For the considered convention shown in Figure 3(b), a positive change in angle β_i will cause a negative change in the length of wire i. Using the backward difference method, $\ddot{\beta}_i$ is approximated as

$$\ddot{\beta}_i(t_k) = \frac{\dot{\beta}_i(t_k) - \dot{\beta}_i(t_{k-1})}{\Delta t} \tag{5}$$

where $\Delta t = t_k - t_{k-1}$ is the time step; the time index k corresponds to the iteration number for the time step. Having the tension in the wires and substituting $\dot{\beta}_i$ from equation (4), and $\ddot{\beta}_i$ given by equation (5) into equation (3) the relation between the actuator torques and the velocity of the mobile platform will be

$$\begin{bmatrix} T_1(t_k) \\ \vdots \\ T_n(t_k) \end{bmatrix} = \begin{bmatrix} r_{p_1} & & 0 \\ & \ddots & \\ 0 & & r_{p_n} \end{bmatrix} \boldsymbol{\tau}(t_k) + \begin{bmatrix} \frac{c_{m_1}}{r_{p_1}} & & 0 \\ & \ddots & \\ 0 & & \frac{c_{m_n}}{r_{p_n}} \end{bmatrix} \mathbf{J} \begin{bmatrix} \dot{x} \\ \dot{y} \\ \dot{\varphi} \end{bmatrix} + \frac{1}{\Delta t} \begin{bmatrix} \frac{I_{p_1}}{r_{p_1}} & & 0 \\ & \ddots & \\ 0 & & \frac{I_{p_n}}{r_{p_n}} \end{bmatrix} \left(\mathbf{J}(t_k) \begin{bmatrix} \dot{x}(t_k) \\ \dot{y}(t_k) \\ \dot{\varphi}(t_k) \end{bmatrix} - \mathbf{J}(t_{k-1}) \begin{bmatrix} \dot{x}(t_{k-1}) \\ \dot{y}(t_{k-1}) \\ \dot{\varphi}(t_{k-1}) \end{bmatrix} \right) \tag{6}$$

2.2. Kinematics of the Tool Tip and Trajectory Planning

The material removal is considered in the modelling to investigate the effect of required cutting forces in the redundancy resolution of wire actuated parallel manipulators. Knowledge of the forces and power involved in cutting operations is important in order to select the machine tool with adequate power, determine if the workpiece can withstand the cutting forces without excessive distortion, and to design the machine tools properly in order to avoid damaging the machine elements and maintain the desired tolerances for the finished part, tooling and toolholders, and workholding devices [11].

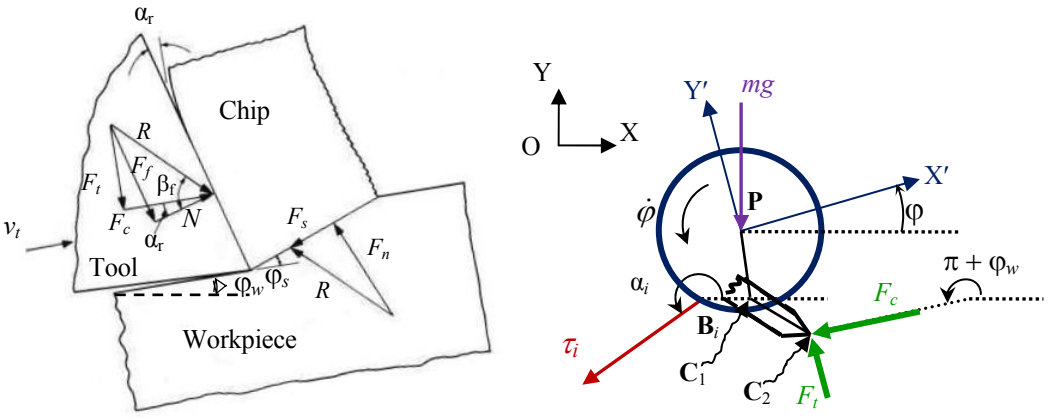

(a) (b)

Figure 4. (a) Force diagram in orthogonal cutting [11], (b) free-body diagram of mobile platform during machining.

The forces acting on the chip in orthogonal cutting are shown in Figure 4(a) and the free-body diagram of the mobile platform during cutting operation is shown in Figure 4(b). Line segment $\overline{C_1C_2}$ represents the cutting tool, where point C_2 corresponds to the tool tip. Figure 5 represents the cutting tool and workpiece variables, as well as the path of the tool tip, C_2, during machining process. Considering Figure 5, the position of the mobile platform can be written as

$$\begin{bmatrix} x \\ y \end{bmatrix} = \begin{bmatrix} x_{C_2} - r_{C_2/P_x} \\ y_{C_2} - r_{C_2/P_y} \end{bmatrix} \tag{7}$$

where the position vector of the contact point C_2 on the cutting tool is $\mathbf{x}_{C_2} = [x_{C_2}, y_{C_2}]^T$ and $\mathbf{r}_{C_2/P} = [r_{C_2/P_x}, r_{C_2/P_y}]^T$ is the position vector of the tool tip with respect to P. Vector $\mathbf{r}_{C_2/P}$ can be replaced as

$$\begin{bmatrix} r_{C_2/P_x} \\ r_{C_2/P_y} \end{bmatrix} = \begin{bmatrix} r_{C_1/P_x} + r_{C_2/C_{1x}} \\ r_{C_1/P_y} + r_{C_2/C_{1y}} \end{bmatrix} \tag{8}$$

where $\mathbf{r}_{C_1/P} = [r_{C_1/P_x}, r_{C_1/P_y}]^T$ is the position vector of the tool attachment point on the mobile platform with respect to P, and $\mathbf{r}_{C_2/C_1} = [r_{C_2/C_{1x}}, r_{C_2/C_{1y}}]^T$ represents the position vector of the tool.

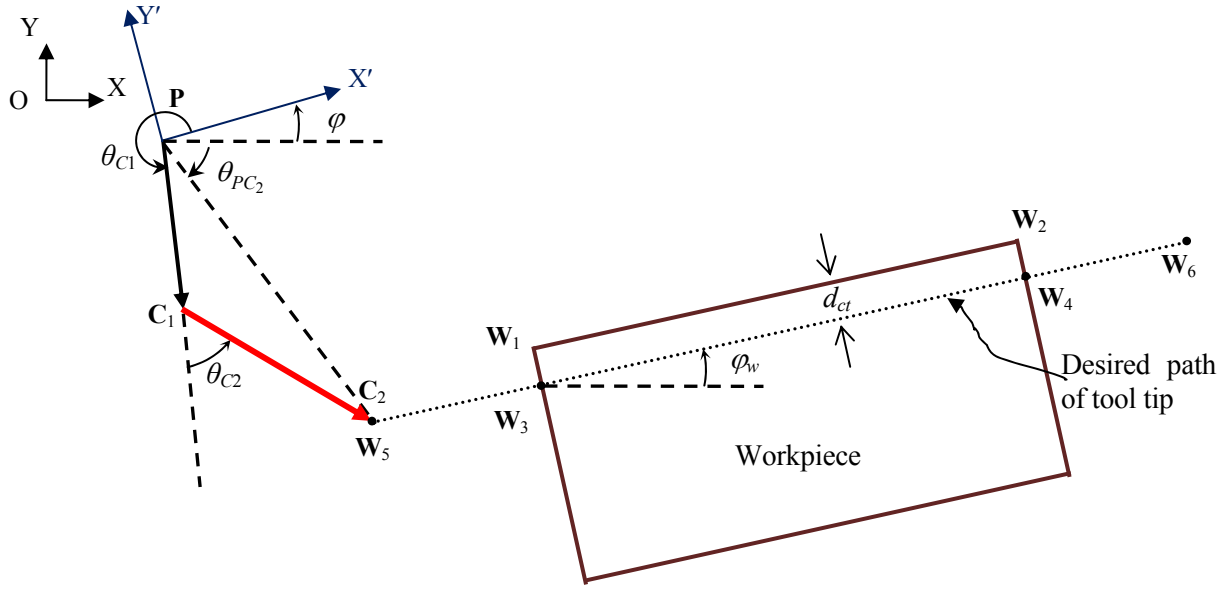

Figure 5. Schematic illustration of cutting tool, workpiece and desired path of tool tip.

Considering Figure 5 and equation (7), the desired trajectory of the mobile platform is determined for a given orientation of the platform, φ, desired cutting trajectory of the workpiece, $\mathbf{x}_{C_2}$, depth of cut, d_{ct}, tool attachment point on the mobile platform, C_1, distance between C_1 and C_2, r_{C_2/C_1}, and the orientation of the position vector $\mathbf{r}_{C_2/C_1}$. Using the kinematic variables shown in Figure 5, equation (7) is rewritten as

$$\begin{bmatrix} x \\ y \end{bmatrix} = \begin{bmatrix} x_{C_2} - r_{C_2/P}\cos(\theta_{PC_2}) \\ y_{C_2} - r_{C_2/P}\sin(\theta_{PC_2}) \end{bmatrix} \tag{9}$$

where θ_{PC_2} is the orientation of the position vector $\mathbf{r}_{C_2/P}$ obtained as below using the four-quadrant inverse tangent and the trigonometry such that $0 \le \theta_{PC_2} \le 2\pi$

$$\theta_{PC_2} = 2\tan^{-1}\left(\frac{r_{C_2/P_y}}{\sqrt{(r_{C_2/P_x}^2 + r_{C_2/P_y}^2)} + r_{C_2/P_x}}\right) \tag{10}$$

For the inverse velocity solution of equation (1) and the dynamic force and moment balances of equation (2), it is required to have the velocity and acceleration of the mobile platform. Differentiating equation (9) results in

$$\begin{bmatrix}\dot{x}\\ \dot{y}\end{bmatrix} = \begin{bmatrix}\dot{x}_{C_2} + r_{C_2/P}\dot{\varphi}\sin(\theta_{PC_2})\\ \dot{y}_{C_2} - r_{C_2/P}\dot{\varphi}\cos(\theta_{PC_2})\end{bmatrix} \tag{11}$$

It should be noted that the rate of change of θ_{PC_2}, $\dot{\theta}_{PC_2}$, is equal to the angular velocity of the mobile platform, $\dot{\varphi}$. Equation (11) can be used in equation (1) for the inverse velocity analysis. The acceleration of the mobile platform is obtained by differentiating equation (11) as

$$\begin{bmatrix}\ddot{x}\\ \ddot{y}\end{bmatrix} = \begin{bmatrix}\ddot{x}_{C_2} + r_{C_2/P}\ddot{\varphi}\sin(\theta_{PC_2}) + r_{C_2/P}\dot{\varphi}^2\cos(\theta_{PC_2})\\ \ddot{y}_{C_2} - r_{C_2/P}\ddot{\varphi}\cos(\theta_{PC_2}) + r_{C_2/P}\dot{\varphi}^2\sin(\theta_{PC_2})\end{bmatrix} \tag{12}$$

The mobile platform acceleration derived using equation (12) can then be substituted into equation (2) for the inverse dynamic analysis.

As an example path planning procedure, an oblique cutting surface can be used for the machining operation, as depicted in Figure 5. Points W_1 and W_2 correspond to the edge corners of the cutting surface of the workpiece. W_3 and W_4 are, respectively, the contact points at which the cutting process starts and ends. W_5 and W_6 refer to the initial and final positions of the tool tip, respectively. The dashed line between W_5 and W_6 represents the desired path of the tool tip. Considering the depth of cut, d_{ct}, the cutting path is chosen to be a line passing through points W_3 and W_4. The cutting trajectory can be determined using the initial and final boundary conditions of $\mathbf{x}_{C_2}$ and its derivatives. For trajectory planning, the following procedure is undertaken. For a linear path, coordinates of W_3 and W_4 are determined as

$$\begin{bmatrix}x_{W_{j+2}}\\ y_{W_{j+2}}\end{bmatrix} = \begin{bmatrix}x_{W_j} + d_{ct}\sin\varphi_w\\ y_{W_j} - d_{ct}\cos\varphi_w\end{bmatrix}, \quad j = 1, 2 \tag{13}$$

where φ_w is the slope of the desired linear path as shown in Figure 5. Given the distances between W_3 and W_5, r_{W_5/W_3}, and between W_4 and W_6, r_{W_6/W_4}, as well as using equation (13), the initial and final positions of the tool tip are respectively obtained as

$$\begin{bmatrix}x_{W_5}\\ y_{W_5}\end{bmatrix} = \begin{bmatrix}x_{W_3} - r_{W_5/W_3}\cos\varphi_w\\ y_{W_3} - r_{W_5/W_3}\sin\varphi_w\end{bmatrix} \tag{14}$$

and

$$\begin{bmatrix}x_{W_6}\\ y_{W_6}\end{bmatrix} = \begin{bmatrix}x_{W_4} + r_{W_6/W_4}\cos\varphi_w\\ y_{W_4} + r_{W_6/W_4}\sin\varphi_w\end{bmatrix} \tag{15}$$

Moreover, the geometric representation of the cutting path (i.e., a line passing through W_3, W_4, W_5, and W_6) is given by

$$y_{C_2} = \frac{y_{W_5} - y_{W_6}}{x_{W_5} - x_{W_6}}x_{C_2} + \frac{x_{W_5}y_{W_6} - x_{W_6}y_{W_5}}{x_{W_5} - x_{W_6}} \tag{16}$$

Thus, depending on the number of boundary conditions of the cutting trajectory, a polynomial equation is selected for the x component of the trajectory, x_{C_2}. Then, using equation (16), the cutting trajectory in y direction, y_{C_2}, is determined.

2.3. Cutting Forces and Power in Orthogonal Cutting

As has been shown by Merchant [12], the following force relationship can be written considering the force diagram shown in Figure 4(a)

$$F_t = F_c \tan(\beta_f - \alpha_r) \tag{17}$$

where F_t is the thrust force acting in the direction normal to the cutting velocity (i.e., perpendicular to the workpiece), F_c is the cutting force acting in the direction of the cutting speed $\mathbf{v}_t$ supplying the energy for cutting, β_f is the friction angle, and α_r is the rake angle as shown in Figure 4(a). The relationship between the friction angle β_f and the coefficient of kinetic friction μ_k in cutting is given as

$$\begin{aligned} \mu_k &= F_f / N = \tan\beta_f \\ &= \frac{F_t + F_c \tan\alpha_r}{F_t - F_c \tan\alpha_r} \end{aligned} \tag{18}$$

where F_f is the friction force along the tool, and N is the normal component of the resultant force R that the tool exerts on the chip. The friction coefficient μ_k in metal cutting ranges from about 0.5 to 2.0 [11].
The power input in cutting is

$$P_c = F_c v_t \tag{19}$$

where v_t is the cutting speed. The total specific energy for cutting, u_t, is

$$u_t = \frac{P_c}{w_c d_{ct} v_t} \tag{20}$$

where w_c is the width of cut and d_{ct} is the depth of cut as shown in Figure 2(b). Replacing the power input P_c in equation (20) with P_c in equation (19), the cutting force F_c is obtained as

$$F_c = w_c d_{ct} u_t \tag{21}$$

Because of the many factors involved, the reliable prediction of cutting forces and power is still based largely on experimental data [11], such as those given in Table 1. The wide range of values in Table 1 corresponds to differences in strength within each material group and various other factors, such as friction, use of cutting fluids, and processing variables [11]. The sharpness of the tool tip also affects forces and power; the duller the tool, the higher are the forces and power required.

Table 1. Approximate energy requirements in cutting operations (at drive motor, corrected for 80% efficiency; multiply by 1.25 for dull tools) [11].

Material	**Specific Energy Ws/mm^3**	**Material**	**Specific Energy Ws/mm^3**
Aluminium alloys	0.4-1.1	Nickel alloys	4.9-6.8
Cast irons	1.6-5.5	Refractory alloys	3.8-9.6
Copper alloys	1.4-3.3	Stainless steels	3.0-5.2
High-temperature alloys	3.3-8.5	Steels	2.7-9.3
Magnesium alloys	0.4-0.6	Titanium alloys	3.0-4.1

Given the width of cut w_c, depth of cut d_{ct}, and using the experimental data given in Table 1, the cutting forces can be predicted using equation (21).

2.4. Contact Force Modelling in Orthogonal Cutting

Using the obtained kinematic results for the velocity and acceleration of the mobile platform, the inverse dynamics of the manipulator represented by equation (2) can be analysed.
Considering Figure 4(b), in the absence of any other external force/moment, $\mathbf{F}_{ext}$ and M_{ext_z} can be written as

$$\mathbf{F}_{ext} = \mathbf{F}_c + \mathbf{F}_t \tag{22}$$

and

$$M_{ext_z} = F_t r_{C_2/P} \cos(\varphi_w - \theta_{PC_2}) - F_c r_{C_2/P} \sin(\varphi_w - \theta_{PC_2}) \operatorname{sgn}(v_{C_2}) \tag{23}$$

where the velocity of point C_2 is $v_{C_2} = \sqrt{(\dot{x}_{C_2}^2 + \dot{y}_{C_2}^2)}$, and $\operatorname{sgn}(v_{C_2})$ is a signum function. Considering equation (17), equation (2) is written as

$$\mathbf{J}^T [\tau_1 \dots \tau_n]^T = \mathbf{M}\ddot{\mathbf{x}} - \mathbf{g} - F_c \mathbf{c} \tag{24}$$

where $\mathbf{c}$ is

$$\mathbf{c} = \begin{bmatrix} -\operatorname{sgn}(v_{C_2}) \cos\varphi_w - \tan(\beta_f - \alpha_r) \sin\varphi_w \\ -\operatorname{sgn}(v_{C_2}) \sin\varphi_w + \tan(\beta_f - \alpha_r) \cos\varphi_w \\ r_{C_2/P} \tan(\beta_f - \alpha_r) \cos(\varphi_w - \theta_{PC_2}) - r_{C_2/P} \sin(\varphi_w - \theta_{PC_2}) \operatorname{sgn}(v_{C_2}) \end{bmatrix} \tag{25}$$

Considering the minimum and maximum allowable tension in the wires, $\tau_{\min}$ and $\tau_{\max}$, respectively, the solution of equation (24) is given by

$$\begin{gathered} [\tau_1 \dots \tau_n]^T = \boldsymbol{\tau}_p + \boldsymbol{\tau}_h \\ 0 \le \tau_{\min} \le \tau_i \le \tau_{\max} \end{gathered} \tag{26}$$

where the minimum norm (particular) solution, $\boldsymbol{\tau}_p$, is

$$\boldsymbol{\tau}_p = \mathbf{J}^{T\#} (\mathbf{M}\ddot{\mathbf{x}} - \mathbf{g} - F_c \mathbf{c}) \tag{27}$$

and the homogeneous solution,$\boldsymbol{\tau}_h$, is

$$\boldsymbol{\tau}_h = (\mathbf{I} - \mathbf{J}^{T\#} \mathbf{J}^T)\mathbf{k} \tag{28}$$

The generalized inverse of the transposed Jacobian, $\mathbf{J}^T$, is $\mathbf{J}^{T\#} = \mathbf{J}(\mathbf{J}^T\mathbf{J})^{-1}$. If $\mathbf{J}^T$ has full row-rank, then $\mathbf{J}^{T\#}$ is invariant to the choice of any weighting metric, e.g., refer to Doty et al. [13]. Therefore, using a weighting metric will not be required.

The homogeneous solution, $\boldsymbol{\tau}_h$, maps the free vector $\mathbf{k}$ to the null space of $\mathbf{J}^T$. The homogeneous solution is interpreted as a portion of wire tensions that result in zero change in the forces/moments at the mobile platform. To simplify equation (26), $\boldsymbol{\tau}_h$ in equation (28) could be written as

$$\boldsymbol{\tau}_h = \mathbf{N}\boldsymbol{\lambda} \tag{29}$$

where $\mathbf{N}$ is a matrix that its columns correspond to the orthonormal basis for the null space of $\mathbf{J}^T$ and may be determined using the singular value decomposition, and $\boldsymbol{\lambda}$ is an arbitrary vector.

Considering the particular solution $\boldsymbol{\tau}_p$, when τ_{p_i} is negative or if the maximum tension limit is violated, using the actuation redundancy, the tension in the wires is modified satisfying the tension constraints.

Therefore, considering $\boldsymbol{\tau}_p$, the minimum norm solution of $\boldsymbol{\tau}$, in equation (24), if the desired tension in wire i is τ_{m_i}, τ_i is replaced with τ_{m_i} as

$$\tau_i = \tau_{m_i} = \mathbf{S}^T [\tau_1 \cdots \tau_i \cdots \tau_n]^T \tag{30}$$

where $\mathbf{S}$ is a sparse $n\times1$ array in which only ith element, corresponding to the wire with different tension, has a value of 1. Substituting the solution of wire tensions given by equation (26) into equation (30) results in

$$\tau_i = \tau_{m_i} = \mathbf{S}^T \boldsymbol{\tau}_p + \mathbf{S}_N \mathbf{k} \tag{31}$$

where $\mathbf{S}_N = \mathbf{S}^T(\mathbf{I} - \mathbf{J}^{T\#}\mathbf{J}^T)$ and it corresponds to the ith row of $(\mathbf{I} - \mathbf{J}^{T\#}\mathbf{J}^T)$. The minimum norm arbitrary vector $\mathbf{k}$ is then obtained as

$$\mathbf{k} = \mathbf{S}_N^{\#} \tau_{m_i} - \mathbf{S}_N^{\#} \mathbf{S}^T \mathbf{J}^{T\#} \left(\mathbf{M}\ddot{\mathbf{x}} - \mathbf{g} - F_c \mathbf{c}\right) \tag{32}$$

where $\mathbf{S}_N^{\#} = \mathbf{S}_N^T (\mathbf{S}_N \mathbf{S}_N^T)^{-1}$ is the generalized inverse of the ith row of $(\mathbf{I} - \mathbf{J}^{T\#}\mathbf{J}^T)$. Given the pose of the mobile platform, a feasible solution for $\mathbf{k}$ is characterized by a convex region bounded by $2n$ linear inequalities on the elements of $\mathbf{k}$ considering the inequality constraints of equation (26). On condition that the feasible region of each element of $\mathbf{k}$ is not empty, there exists a solution for wire tensions such that $[F_{ext_x}, F_{ext_y}, M_{ext_z}] = F_c \mathbf{c}$. Otherwise, the tension constraints cannot be satisfied. As an example, if $\tau_{m_i} = 0$, then $\mathbf{k} = -\mathbf{S}_N^{\#} \tau_{p_i}$. If a solution exists for $\mathbf{k}$, it can be concluded that the given pose is within the workspace.

The procedure can be generalized when k wires have different tensions, the minimum norm arbitrary vector $\mathbf{k}$ is calculated as

$$\mathbf{k} = \mathbf{S}_{N_k}^{\#} \left[\tau_{m_1} \ldots \tau_{m_k}\right]^T - \mathbf{S}_{N_k}^{\#} \mathbf{S}_k^T \mathbf{J}^{T\#} \left(\mathbf{M}\ddot{\mathbf{x}} - \mathbf{g} - F_c \mathbf{c}\right) \tag{33}$$

where $\mathbf{S}_k$ is a sparse matrix with n rows and $k \le r$ columns in which only elements $s_{i,k} = 1$, the degree of actuation redundancy is $r = n - m$, m is the dimension of the task space, index i corresponds to the wire with different tension, $\mathbf{S}_{N_k} = \mathbf{S}_k^T (\mathbf{I} - \mathbf{J}^{T\#}\mathbf{J}^T)$, and $\mathbf{S}_{N_k}^{\#} = \mathbf{S}_{N_k}^T (\mathbf{S}_{N_k} \mathbf{S}_{N_k}^T)^{-1}$.

It should be noted that for r degrees of redundancy, r extra constraints (e.g., desired tensions in r wires) result in a closed form solution for vector $\mathbf{k}$ (only if $\mathbf{k}$ has a feasible region). Therefore, if there are more than r desired constraints on specific wire tensions, there may not be a solution for vector $\mathbf{k}$.
Once wire tensions are calculated, a suitable wire is selected considering the maximum required wire tension and the safety factor.

3. SIMULATION

In this section, the simulation results of redundancy resolution of the planar wire-actuated manipulator, shown in Figure 2(a), are presented. For the simulation, the anchor positions are $\{\mathbf{a}_1, \mathbf{a}_2, \mathbf{a}_3, \mathbf{a}_4\} = \{[-1, -0.75]^T, [1, -0.75]^T, [1, 0.75]^T, [-1, 0.75]^T\}$ (units in meters), and the angular positions of wire attachment points on the mobile platform with respect to the moving frame are defined by $\{\theta_1, \theta_2, \theta_3, \theta_4\} = \{225, 315, 45, 135\}$ (units in degrees). The mass m, moment of inertia I_z, and radius $r_{Bi/P}$ of the mobile platform are respectively 2 kg, 0.0144 kg.m^2, and 0.125 m. The moment of inertia of each spool I_{pi}, the radius of each spool r_{pi}, and the viscous damping coefficient at each motor shaft c_{mi} are respectively 0.0008 kg.m^2, 0.05 m, and 0.01 Nms. Considering the convention shown in Figure 3(b), all spool angles β_i are defined to be zero initially. The manipulator is designed to be used in cutting of Aluminum alloys with minimum required total specific energy of 0.4 Ws/mm^3 as given in Table 1. The width of cut w_c, the depth of cut d_{ct}, the coefficient of kinetic friction μ_k, and the rake angle α_r are respectively 4 mm, 1 mm, 0.5, and 10 deg. Considering Figure 5, the angles θ_{C1}, θ_{C2} and φ_w are respectively 240 deg and 50 deg. The distance $r_{C_1/P}$

is 0.12 m, r_{C_2/C_1} is 0.12 m, and the x and y coordinates of points W_1 and point W_2 are respectively $[-0.25, -0.4]^T$ and $[0.5, -0.3]^T$. The distances r_{W_5/W_3} r_{W_6/W_4} are equally 0.2 m.

The desired trajectories for x_{C_2} and φ are chosen to be fifth order polynomials satisfying eighteen initial and final boundary conditions of both trajectories and their derivatives. The initial and final boundary conditions $\left(x_{C_2}, \dot{x}_{C_2}, \ddot{x}_{C_2}, \varphi, \dot{\varphi}, \ddot{\varphi}\right)$ are $(x_{W_5}, 0, 0, 0, 0, 0)_0$ and $(x_{W_6}, 0, 0, 2\text{ deg}, 0, 0)_f$, respectively, with $t \in [0, 10]$ s and time step of $\Delta t = 0.01$ s. Coordinates x_{W_5} and x_{W_6} are calculated using equation (14) and equation (15), accordingly. The cutting trajectory in y direction, y_{C_2}, is determined using equation (16). The minimum allowable tension of each wire is $\tau_{\min} = 2$ N. With four wires, the constraint function in equation (26) is reduced to eight linear inequalities in terms of $\boldsymbol{\lambda}$ given in equation (29), where $\boldsymbol{\lambda}$ is reduced to a scalar.

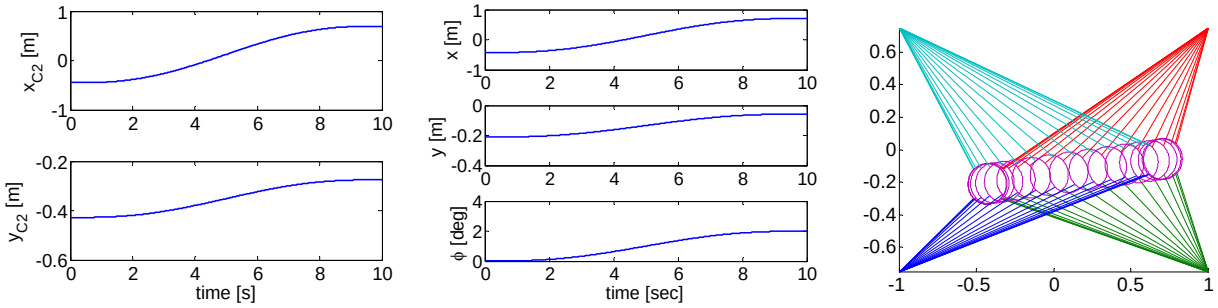

(a) (b) (c)

Figure 6. (a) Tool tip trajectory, (b) trajectory of mobile platform, (c) configuration of mobile platform.

Figure 6(a), (b) and (c) show the tool tip trajectory, the mobile platform trajectory, and the configuration of the mobile platform along the given trajectory, respectively.

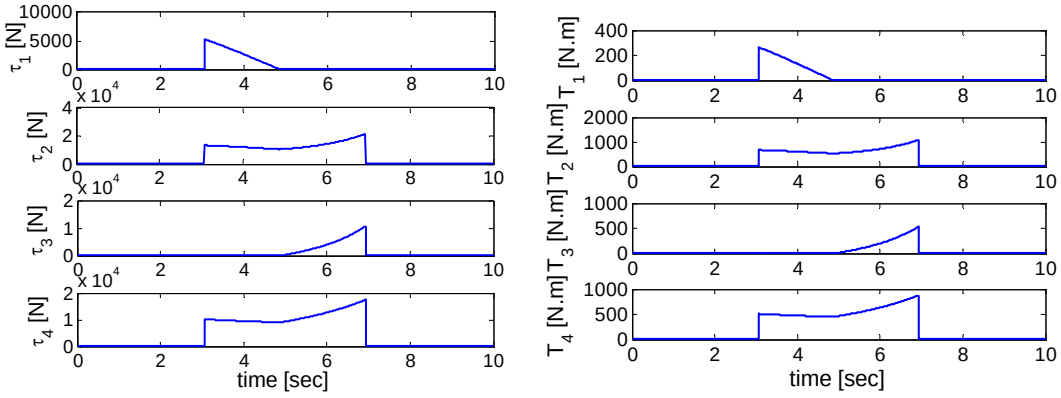

(a) (b)

Figure 7. (a) Tension in wires, (b) actuator torques.

Figure 7(a) illustrates the tension histories. It can be seen that the maximum wire tension during cutting process is approximately 2×10^4 N. Thus, considering a safety factor of 3, a wire rope with a minimum breaking strength of 6×10^4 N should be selected. For example, a zinc-plated rope with 3/8 in (9.5 mm) diameter and 14400 lbs (6532 kg) breaking strength is suitable for this application. These specifications were selected from McMaster-Carr Supply Company [14]. Substituting the wire tensions and the velocity of mobile platform into equation (6) results in the actuator torques shown in Figure 7(b). Considering Figure 7(a) and (b), the machining operation starts at $t = 3.06$ s and finishes at $t = 6.94$ s.

4. SUMMARY AND CONCLUSIONS

In the work presented, the kinematics and dynamics of wire-actuated parallel manipulators was investigated in machining applications. Considering the machining surface and the depth of cut, the trajectory of the mobile platform was defined given the desired initial and final position, velocity and acceleration of the tool tip. The actuation redundancy of the manipulator was resolved while minimizing the wire tensions and following the machining trajectory with minimum positive tension in each wire. The infinite solutions for wire tensions were utilized to identify a vector of wire tensions providing the required cutting force based on the knowledge of the required machining power. The simulation of a 3-DOF planar wire-actuated parallel manipulator was developed satisfying machining requirements.

This paper considered using wire-actuated manipulators in machining applications and made recommendations for the diameter and material of the wires to support the determination of wire tensions.

REFERENCES

[1] S. Kawamura, K. Hitoshi and W. Choe, "High-speed manipulation by using parallel wire-driven robots," *Robotica,* vol. 18, pp. 13-21, 2000.

[2] W. Choe, K. Hitoshi, K. Katsuta and S. Kawamura, "A design of parallel wire driven robots for ultrahigh speed motion based on stiffness analysis," *Proceedings of the Japan/USA Symposium on Flexible Automation,* pp. 159-166, 1996.

[3] D. McColl and L. Notash, "Configuration and workspace analysis of planar wire-actuated parallel manipulators," *Proceedings of the 17th CISM-IFToMM Symp. Robot Design, Dynamics, and Control (RoManSy),* Japan, 8 pages, 2008.

[4] D. McColl and L. Notash, "Extension of antipodal theorem to workspace analysis of planar wire-actuated manipulators," *Proc. of 5th IFToMM Int. Workshop on Computational Kinematics,* Duisburg, Germany, 8 pages, 2009.

[5] R. L. Williams II and P. Gallina, "Translational Planar Cable-Direct-Driven Robots," *Journal of Intelligent and Robotic Systems,* vol. 37, pp. 69-96, 2003.

[6] R. L. Williams II, P. Gallina and J. Vadia, "Planar Translational Cable-Direct-Driven Robots," *Journal of Robotic Systems,* vol. 20, pp. 107-120, 2003.

[7] S.-R. Oh and S. K. Agrawal, "Cable Suspended Planar Robots with Redundant Cables: Controllers with Positive Tensions," *IEEE Transactions on Robotics,* vol. 21, pp. 457-465, 2005.

[8] L. Notash and A. Kamalzadeh, "Inverse dynamics of wire-actuated parallel manipulators with a constraining linkage," *Mechanism and Machine Theory,* vol. 42, pp. 1103-1118, 2007.

[9] M. Agahi and L. Notash, "Redundancy resolution of wire-actuated parallel manipulators," *Special Edition of the Transactions of the Canadian Society of Mechanical Engineers*, vol. 33, no. 4, pp. 561-575, 2009.

[10] X. Diao and O. Ma, "Vibration analysis of cable-driven parallel manipulators," *Multibody System Dynamics*, vol. 21, no. 4, pp. 347-360, 2009.

[11] S. Kalpakjian, "Fundamentals of Cutting," in *Manufacturing Engineering and Technology,* 3rd ed., Addison Wesley, pp. 590-612, 1995.

[12] M. E. Merchant, "Mechanics of the Metal Cutting Process. I. Orthogonal Cutting and a Type 2 Chip," *Journal of Applied Physics*, vol. 16, no. 5, pp. 267-275, 1945.

[13] K. I. Doty, C. Melchiorri and C. Bonivento, "A Theory of Generalized Inverses Applied to Robotics," *International Journal of Robotics Research,* vol. 12, pp. 1-19, 1995.

[14] Anonymous, "Wire Rope," Available: http://www.mcmaster.com/#wire-rope/=atr880, Accessed April 18, 2011.